

## RESEARCH ARTICLE

10.1002/2014JD022254

## Special Section:

Fast Physics in Climate Models: Parameterization, Evaluation and Observation

This article is a companion to *Li et al.* [2014] doi:10.1002/2014JD022245.

## Key Points:

- Derive scale-aware forcing from fine-resolution data assimilation analyses
- Characterize subgrid-scale dynamic components in large-scale forcing
- Present a set of single-column model sensitivity simulations

## Correspondence to:

S. Feng,  
sfeng@jiffresse.ucla.edu;  
Sha.Feng@jpl.nasa.gov

## Citation:

Feng, S., Z. Li, Y. Liu, W. Lin, M. Zhang, T. Toto, A. M. Vogelmann, and S. Endo (2015), Development of fine-resolution analyses and expanded large-scale forcing properties: 2. Scale awareness and application to single-column model experiments, *J. Geophys. Res. Atmos.*, 120, doi:10.1002/2014JD022254.

Received 3 JUL 2014

Accepted 13 DEC 2014

Accepted article online 17 DEC 2014

## Development of fine-resolution analyses and expanded large-scale forcing properties: 2. Scale awareness and application to single-column model experiments

Sha Feng<sup>1,2</sup>, Zhijin Li<sup>1,2</sup>, Yangang Liu<sup>3</sup>, Wuyin Lin<sup>3</sup>, Minghua Zhang<sup>4</sup>, Tami Toto<sup>3</sup>, Andrew M. Vogelmann<sup>3</sup>, and Satoshi Endo<sup>3</sup><sup>1</sup>Joint Institute for Regional Earth System Science and Engineering, University of California, Los Angeles, California, USA, <sup>2</sup>Jet Propulsion Laboratory, California Institute of Technology, Pasadena, California, USA, <sup>3</sup>Environmental Sciences Department, Brookhaven National Laboratory, Upton, New York, USA, <sup>4</sup>Stony Brook University, Stony Brook, New York, USA

**Abstract** Fine-resolution three-dimensional fields have been produced using the Community Gridpoint Statistical Interpolation (GSI) data assimilation system for the U.S. Department of Energy's Atmospheric Radiation Measurement Program (ARM) Southern Great Plains region. The GSI system is implemented in a multiscale data assimilation framework using the Weather Research and Forecasting model at a cloud-resolving resolution of 2 km. From the fine-resolution three-dimensional fields, large-scale forcing is derived explicitly at grid-scale resolution; a subgrid-scale dynamic component is derived separately, representing subgrid-scale horizontal dynamic processes. Analyses show that the subgrid-scale dynamic component is often a major component over the large-scale forcing for grid scales larger than 200 km. The single-column model (SCM) of the Community Atmospheric Model version 5 is used to examine the impact of the grid-scale and subgrid-scale dynamic components on simulated precipitation and cloud fields associated with a mesoscale convective system. It is found that grid-scale size impacts simulated precipitation, resulting in an overestimation for grid scales of about 200 km but an underestimation for smaller grids. The subgrid-scale dynamic component has an appreciable impact on the simulations, suggesting that grid-scale and subgrid-scale dynamic components should be considered in the interpretation of SCM simulations.

## 1. Introduction

In Part I [Li *et al.*, 2014], the first in a series of three papers, data assimilation is used to produce fine-resolution three-dimensional fields of meteorological and other variables for the U.S. Department of Energy's Atmospheric Radiation Measurement Program (ARM) Southern Great Plains (SGP) site. The Community Gridpoint Statistical Interpolation (GSI) data assimilation system is implemented in a multiscale data assimilation (MS-DA) algorithm to manage the difficulties that arise when operating at fine resolution. The GSI system is an operational data assimilation system developed by the National Centers for Environmental Prediction (NCEP). The Weather Research and Forecasting (WRF) model is used and configured at a cloud-resolving resolution of 2 km [Randall *et al.*, 2003].

The ARM established the SGP site in 1992 and has continuously gathered a wide variety of observations since then. The ARM SGP site encompasses the area of a typical global climate model (GCM) grid cell and contains high-resolution surface-based measurements focused on cloud-related fast processes [Stokes and Schwartz, 1994; Ackerman and Stokes, 2003; Mather and Voyles, 2013]. The MS-DA algorithm assimilates ARM measurements along with observations processed by NCEP, particularly radiances from an array of polar-orbiting satellites. The fine-resolution three-dimensional fields generated by the MS-DA were evaluated in Part I and found to be capable of reproducing a mesoscale convective system with its associated clouds and precipitation.

Large-scale forcing has been routinely produced for the SGP site for a variety of applications [e.g., Xie *et al.*, 2004], the most important of which is to drive single-column models (SCMs) for testing physical parameterizations in GCMs. The MS-DA analysis is used to expand the properties of large-scale forcing to include scale-awareness and hydrometeor forcing. In Part III (S. Feng *et al.*, Development of fine-resolution analyses and expanded properties of large-scale forcing. Part III: Hydrometeor forcing and application to single-column model experiments, submitted to *Journal of Geophysical Research*, 2014), we demonstrate the significant impact of hydrometeor forcing on SCM simulations as did Petch and Dudhia [1998]; yet so far, hydrometeor forcing is not

part of existing large-scale forcing products. This paper focuses on characterizing the scale-aware forcing and assesses its impact on SCM simulations.

Here “scale-aware properties” of the large-scale forcing refers to its explicit grid-scale dependence and subgrid-scale dynamic component. The grid-scale dependence has become important to address as GCM grid spacing size, or spatial resolution, has become increasingly fine. The spatial resolutions of current GCMs range from an order of 100 km to an order of 10 km [Intergovernmental Panel on Climate Change (IPCC), 2013]. The large-scale forcing used to drive an SCM must represent the grid scale associated with the GCM, noting that a given GCM can operate at a range of spatial resolutions rather than having a fixed resolution. As we will show in section 3, large-scale forcing fields vary significantly with grid scale, and correspondingly, SCM simulations are sensitive to these variations. Thus, the dependence of large-scale forcing on grid scale must be considered when interpreting SCM simulations.

Generally, the subgrid-scale dynamic component consists of the subgrid-scale vertical flux divergences and horizontal flux divergences that are not parameterized. The nonparameterized component must be included as part of the large-scale forcing, as we will see in section 2. In the latest GCMs, the subgrid-scale vertical fluxes associated with turbulence and convection are parameterized, so we may assume that the significant subgrid-scale vertical fluxes are accounted for in the parameterization. The subgrid-scale horizontal fluxes are also parameterized in GCMs but only partially. Subgrid-scale horizontal fluxes are nonlinear processes that act on the atmospheric flow system via downscale and upscale interactions. Downscale interactions are parameterized by hyperdiffusion ( $\sim \nabla^{2h}$ ). It has been proposed that upscale interactions be parameterized as stochastic forcing to account for the irregular and unpredictable nature of subgrid-scale dynamic processes [e.g., Palmer, 2001; Hoskins et al., 2004]. Stochastic parameterizations are included in some numerical weather prediction models [Buizza et al., 1999; Shutts, 2001], but they are not yet implemented in most GCMs. Thus, it is necessary to include the subgrid-scale horizontal flux divergence in the large-scale forcing.

In the existing large-scale forcing products, the subgrid-scale horizontal flux component is often implicitly included. The standard ARM large-scale forcing generated using the constrained objective variational analysis [Zhang and Lin, 1997] implicitly includes it, although it could be underestimated due to the limited number of grid points used for the line integration to calculate the area-mean flux divergence [Ooyama, 1987]. The large-scale forcing derived from cloud-resolving model simulations by Bechtold et al. [2000] contained the subgrid-scale component as well. We will show that it can be a significant component in large-scale forcing and appreciably impact SCM simulations.

The paper is organized as follows. Section 2 describes the formulation for deriving large-scale forcing and the subgrid-scale dynamic component. Section 3 presents the derived large-scale forcings for different grid scales to examine the scale dependence. Section 4 presents the subgrid-scale dynamic component and quantifies its importance in relation to grid-scale forcing. In section 5, we conduct experiments using the single-column version of the Community Atmospheric Model version 5 (CAM5), known as SCAM5, to demonstrate the sensitivity of SCM simulations to grid-scale size and to the subgrid-scale dynamic component. A summary and discussion is given in section 6.

## 2. Scale-Aware Large-Scale Forcing

Following Part I [Li et al., 2014], the thermodynamic and moisture conservation equation for an SCM can be written in the form:

$$\frac{\partial \bar{T}}{\partial t} = \left( \frac{\partial \bar{T}}{\partial t} \right)_{LS} - \overline{\nabla \cdot \mathbf{V}'T'} - \frac{1}{\gamma_\tau} (\bar{T} - \bar{T}_{LS}) + \frac{\bar{Q}}{c_p} - \left( \frac{\partial \omega' T'}{\partial p} - \frac{\omega' \alpha'}{c_p} \right), \quad (1)$$

$$\frac{\partial \bar{q}}{\partial t} = \left( \frac{\partial \bar{q}}{\partial t} \right)_{LS} - \overline{\nabla \cdot \mathbf{V}'q'} - \frac{1}{\gamma_\tau} (\bar{q} - \bar{q}_{LS}) + \bar{S} - \frac{\partial \omega' q'}{\partial p}, \quad (2)$$

where

$$\left( \frac{\partial \bar{T}}{\partial t} \right)_{LS} = -\bar{\mathbf{V}} \cdot \nabla \bar{T} - \bar{\omega} \left( \frac{\partial \bar{T}}{\partial p} - \frac{\bar{\alpha}}{c_p} \right), \quad (3)$$

$$\left( \frac{\partial \bar{q}}{\partial t} \right)_{LS} = -\bar{\mathbf{V}} \cdot \nabla \bar{q} - \bar{\omega} \frac{\partial \bar{q}}{\partial p}. \quad (4)$$

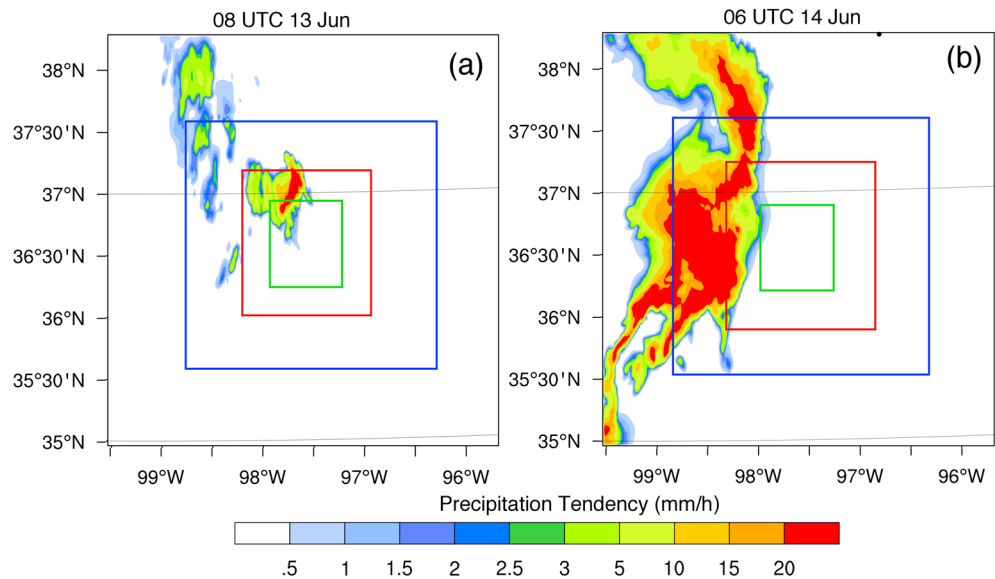


**Figure 1.** The domains used to calculate forcing components. The colored squares denote the following domains: 300 km × 300 km (black), 200 km × 200 km (blue), 100 km × 100 km (red), and 50 km × 50 km (green). All domains are centered on the ARM SGP central facility (36.63°N, 97.49°W). The color-filled contours show the distribution of surface precipitation rate (mm/h) generated from the MS-DA system at (a) 08:00 UTC on 13 June and (b) 06:00 UTC on June 14. The intense precipitation is associated with an MCS.

The variables are defined as follows:  $V$ , horizontal wind;  $\omega$ , vertical  $p$  velocity;  $p$ , pressure;  $p_0$ , surface pressure;  $\alpha$ , specific volume of the air;  $c_p$ , the specific heat at constant volume;  $\nabla$ , the horizontal del operator;  $Q$ , the heating rate;  $S$ , the source of water vapor; and  $\gamma_r$ , the relaxation time scale. The overbar denotes a horizontal average over a given domain.

The second term on the right-hand side in equations (1) and (2) is the subgrid-scale dynamic component; the third represents the relaxation term. Relaxation is linked to the horizontal advection term and in turn is linked to subgrid-scale dynamic term [Randall and Cripe, 1999]. This linkage implies that the subgrid-scale dynamic component and relaxation terms may be dynamically inappropriate to include together in equations (1) and (2). We will further address this topic in section 5.3.

Using domain averages, we can calculate the grid-scale component of each  $T$  forcing and  $q$  forcing as defined by equations (3) and (4), respectively. For simplicity, we call the grid-scale forcing of equation (3) the  $T$  forcing and the grid-scale forcing of equation (4) the  $q$  forcing. Here the subgrid-scale dynamic component is the subgrid-scale horizontal flux only.

The subgrid-scale horizontal and vertical fluxes are not independent but, rather, are related to each other through the continuity equation. The vertical flux consists of a component that is parameterized and a component that is not. Since the primary component of the vertical flux has been parameterized, the subgrid-scale horizontal flux in the large-scale forcing must be included to keep consistency between the subgrid-scale horizontal and vertical fluxes.

### 3. Grid-Scale Forcing

SCMs have been used to test and evaluate physical parameterization schemes as early as two decades ago [e.g., Betts and Miller, 1986]. Since then, GCM resolutions have become increasingly fine, from a few 100 km down to tens of kilometers. The ARM SGP site was initially designed to match the grid scale of GCMs from the late 1980s and early 1990s, covering a domain about 300 km in diameter for which the ARM large-scale forcing product was produced. The observing area for the ARM SGP site has been reduced recently, focusing on a smaller domain comparable to the finer spatial resolutions used in newer GCMs.

The MS-DA analysis offers the flexibility of deriving grid-scale forcing fields for a range of grid sizes. We calculate the grid-scale forcing for grid scales of 300, 200, 100, and 50 km (Figure 1); the domains are,

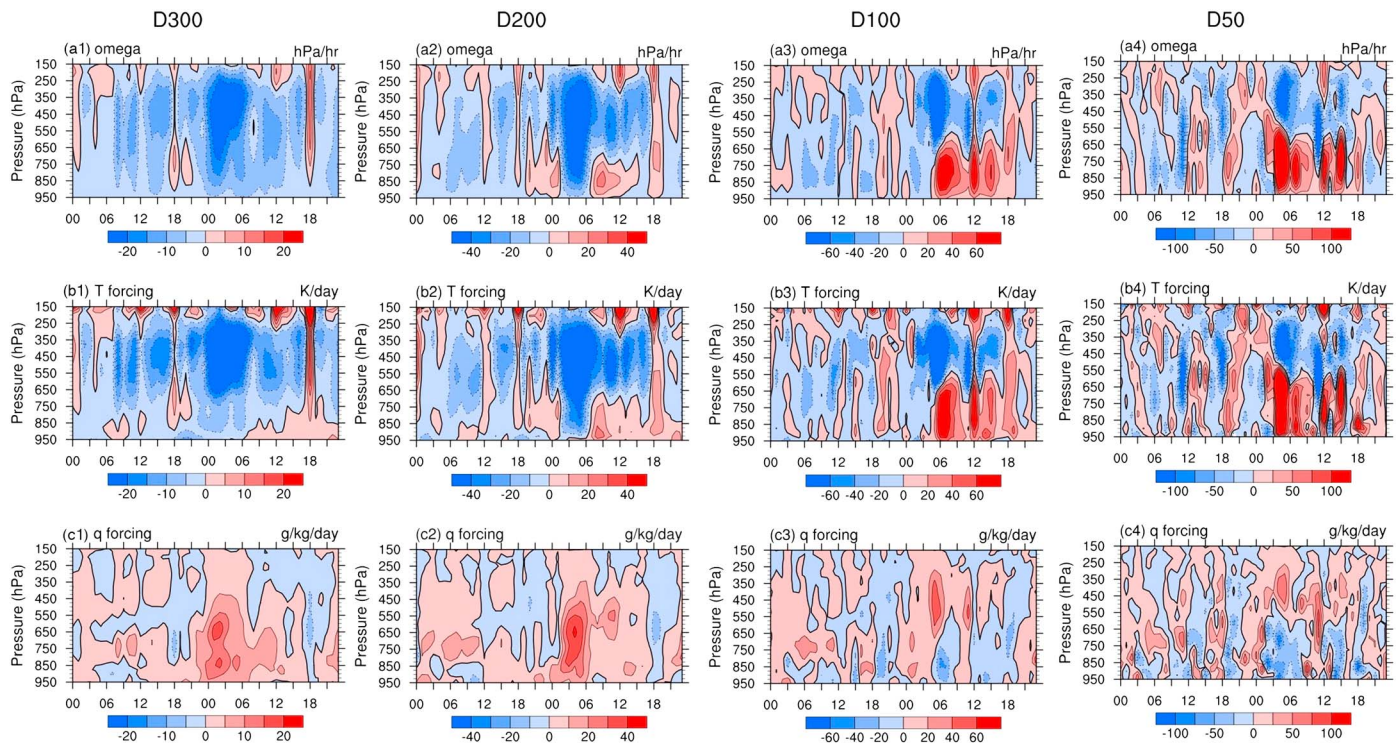


**Figure 2.** (a1–a4) The large-scale (or grid-scale) pressure vertical velocity, (b1–b4)  $T$  forcing, and (c1–c4)  $q$  forcing. Columns display the large-scale forcing fields for each grid scale: D300, D200, D100, and D50. Note the change in color scale with grid size and that the x axis is in UTC time starting at 00:00 UTC on 13 June.

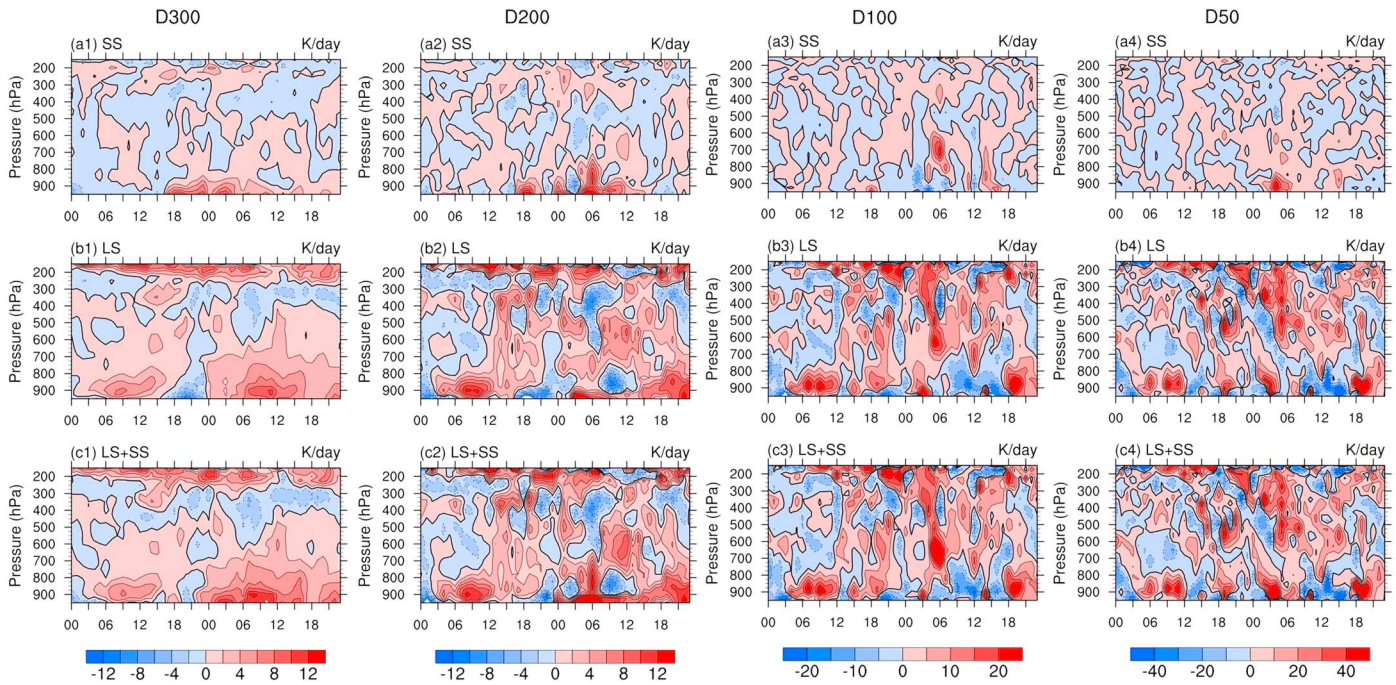
respectively, D300, D200, D100, and D50. By definition, the subgrid-scale dynamic component is the deviation from the domain average, and hence, it is straightforward to calculate the subgrid-scale dynamic component for all domains.

Figure 1 depicts the development of a major precipitation band during a mesoscale convective system (MCS) [Houze, 2004] that occurred from 13 to 15 June 2007. Figure 2 illustrates the differences in large-scale forcing fields associated with the four grid scales. As expected, the vertical velocity and the grid-scale  $T$  and  $q$  forcings increase in terms of temporal variability and intensity as spatial resolution increases. The variability of the grid-scale forcing is associated with the intensification, decay, and movement of the MCS. These features are discussed further in section 4.

#### 4. Subgrid-Scale Dynamic Component

This section characterizes the subgrid-scale dynamic component during the MCS event. Figure 3 displays the temperature subgrid-scale dynamic component (SS), the grid-scale component (LS), and the combined amount (LS + SS) for the four grid scales. The subgrid-scale dynamic component (Figures 3a1–3a4) tends to have large intensities that are primarily confined to the boundary layer. For D100, we also see significant values near 700 hPa around 06:00 UTC on 14 June. There is strong temporal variability, which can be attributed to the related mesoscale activity. A maximum occurs around 06:00 UTC on 14 June, when the MCS reaches its peak intensity between 03:00 UTC and 09:00 UTC on 14 June. Overall, the magnitude of the subgrid-scale dynamic component gets larger for smaller grid scales.

To show the significance of the subgrid-scale dynamic component, we compare it with the corresponding grid-scale horizontal advection, which does not include the subgrid-scale component (Figures 3b1–3b4). For the D300 and D200 domains and in the lower troposphere, the subgrid-scale dynamic component is comparable to the grid-scale counterpart. For the D100 and D50, the overall magnitude of the subgrid-scale component is generally smaller than its grid-scale counterpart, but its magnitude is larger during the intensive convective time period at approximately 06:00 UTC on 14 June.



**Figure 3.** (a1–a4) Subgrid-scale dynamic components for the thermodynamic fields  $\overline{(\nabla \cdot \nabla T)}$  in equation (1) for domains D300, D200, D100, and D50. (b1–b4) The grid-scale horizontal advection  $(-V \cdot \nabla T)$  in equation (3) (c1–c4) and their sum are also given. The label SS denotes subgrid-scale, and LS denotes large-scale (or grid-scale). Note the change in color scale with grid size and that the x axis is in UTC time starting at 00:00 UTC on 13 June.

Figures 4a1–4a4 display the subgrid-scale dynamic component of  $q$  forcing for the four grid scales. Similar to the subgrid-scale dynamic component of  $T$  forcing, the temporal variability in the  $q$  subgrid-scale dynamic component is also concentrated in the lower troposphere and peaks around 06:00 UTC on 14 June. We note that for the smallest grid, D50, the subgrid-scale component tends to have a smaller magnitude. We expect that the importance of the subgrid-scale dynamic component would be further reduced as grid resolution increases. This is consistent with the experience that an increase in GCM resolution generally improves model performance.

To illustrate the relative significance of the subgrid-scale dynamic component, we compare the subgrid-scale dynamic components in Figures 3 and 4 to the total grid-scale forcing in Figure 2. Near the surface or even in the lower troposphere, the subgrid-scale dynamic component could be close to 100% of the magnitude of the total  $T$  forcing and  $q$  forcing for D300, ~60% and ~90% for D200, ~25% and 50% for D100, and ~20% of both for D50, respectively. Thus, the subgrid-scale dynamic component can be a significant component of the total large-scale forcing fields and fundamentally impact SCM simulations as will be shown in the next section.

## 5. Single-Column Model Sensitivity Experiments

Here we examine the sensitivity of SCM simulations to grid-scale and subgrid-scale dynamic components and their relative significance to each other. The SCM experiments are conducted using SCAM5. SCAM5 contains all physical processes used in CAM5 [Neale *et al.*, 2010], which includes the cloud microphysics and macrophysics schemes. Details about microphysical conversions among cloud liquid droplets, ice crystal, rain, and snow can be found in Gettelman *et al.* [2008], Morrison and Gettelman [2008], Gettelman *et al.* [2010], and Song *et al.* [2013].

To quantify the sensitivity of SCAM5 simulations to the subgrid-scale dynamic component, four experiments are conducted for each of the four grid scales (D300, D200, D100, and D50). These experiments are summarized in Table 1 and are conducted with and without relaxation. When analyzing the experiments, we focus primarily on the sensitivity of simulated precipitation and cloud fraction to the grid-scale and to the subgrid-scale dynamic components. The simulated precipitation and cloud fraction are compared to observations. The precipitation data are from the ABRFC (Arkansas-Red Basin River Forecast Center, available

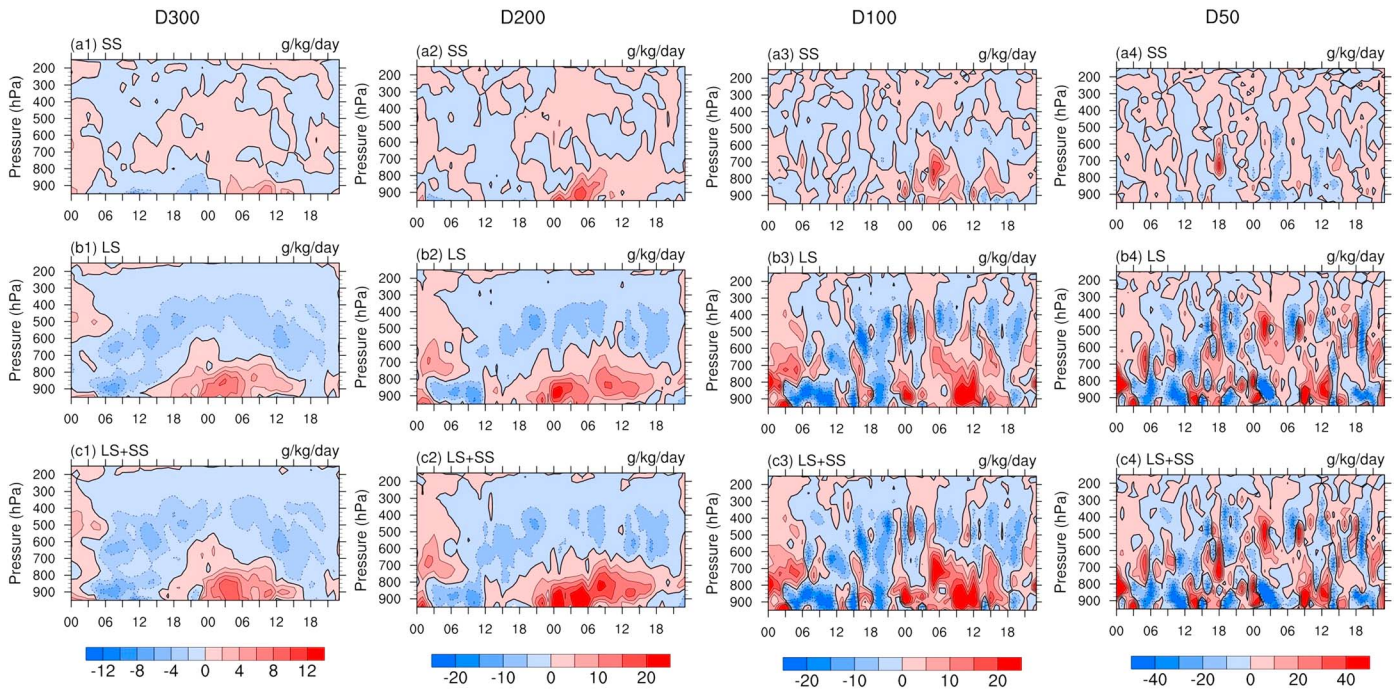


**Figure 4.** Subgrid-scale dynamic components for the moisture fields  $\overline{(\nabla \cdot V'q)}$  in equation (2) for (a1–a4) domains D300, D200, D100, and D50. (b1–b4) The grid-scale horizontal advection  $(-\nabla \cdot \nabla \bar{q})$  in Eq. (4)) and (c1–c4) their sum are also given. The label SS denotes subgrid scale, and LS denotes large scale (or grid scale). Note the change in color scale with grid size and that the x axis is in UTC time starting at 00:00 UTC on 13 June.

at <http://www.arm.gov/data/vaps/abrfc>. The data consist of 4 km hourly precipitation estimates from a combination of WSR-88D Next Generation Weather Radar precipitation estimates and rain gauge reports. We use hourly cloud fractional occurrence over the ARM SGP Central Facility from the Active Remote Sensing of Clouds [Clothiaux et al., 2000, 2001], which is determined from measurements made by the Millimeter Wavelength Cloud Radar and Micropulse Lidar and is as provided in the ARM Best Estimate Data Products (ARMBE) [Xie et al., 2010]. Note that observations used in the evaluation were not assimilated in the MS-DA analysis.

### 5.1. Derived Forcing for Different Grid Scales

Figure 5 presents the domain-averaged simulated precipitation rate from the SCAM5 experiments, the MS-DA analysis, and the domain-averaged precipitation rate from observations. Before discussing the SCAM5 results, we look at the precipitation from the MS-DA. For all four grid scales, the MS-DA realistically reproduces the timing of the main convective precipitation event; the magnitude is realistically represented at D300 but overestimated for the other domains. Given that ABRFC precipitation is not assimilated to the MS-DA system, the realistic timing of the simulated MS-DA precipitation occurs as the result of proper internal balances in the MS-DA analysis.

We first compare the MS-DA and SCAM5-simulated precipitation. For the case of LS\_norelax (dashed blue), where the grid-scale forcing component is used without relaxation, the precipitation rates are

**Table 1.** SCAM5 Experiments<sup>a</sup>

Experiment	Forcing Component	Relaxation
LS_norelax	Grid-scale component only	No relaxation
LS_3hrelax	Grid-scale component only	3 h relaxation
LS+SS_norelax	Grid-scale and subgrid-scale components	No relaxation
LS+SS_3hrelax	Grid-scale and subgrid-scale components	3 h relaxation

<sup>a</sup>The forcing component for each experiment includes, by default, vertical advection of temperature and moisture. The following only highlights the differences between the experiments.

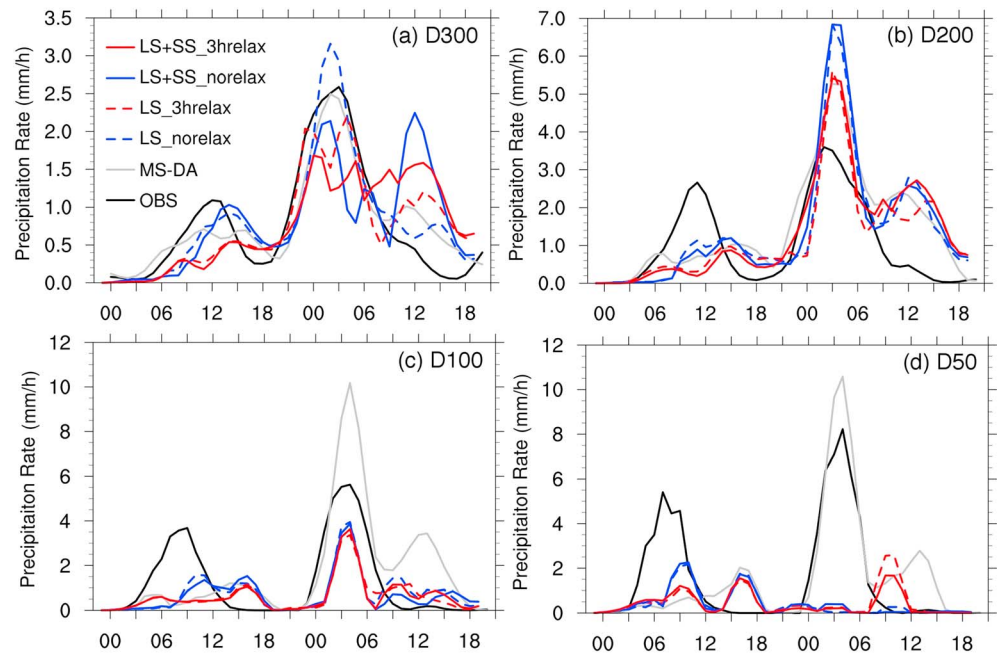


**Figure 5.** SCAM5-simulated precipitation rates for (a) D300, (b) D200, (c) D100, and (d) D50. There are four experiments for each grid scale: large-/grid-scale forcing components without a relaxation (LS\_norelax, dashed blue), large-/grid-scale forcing components with 3 h relaxation (LS\_3hrelax, dashed red), large-/grid- plus subgrid-scale dynamic forcing components without a relaxation (LS+SS\_norelax, solid blue), and large/grid- plus subgrid-scale dynamic forcing components with 3 h relaxation (LS+SS\_3hrelax, solid red). The domain-averaged surface precipitation rates from the ABRFC observations (black solid line) and from the MS-DA system (gray solid line) are also given. Note that the x axis is in UTC time starting at 00:00 UTC on 13 June.

comparable to observations for the D300 grid scale, are overestimated for D200, and are underestimated for D100 and D50. In fact, the largest precipitation event does not even occur for D50. The parameterization in SCAM5 seems best suited for 300 km grid scale, highlighting the importance of the scale dependence of large-scale forcing. For the case of LS\_3hrelax (dashed red), there is a clear reduction of precipitation rate during the convective period for D300 and D200 compared to LS\_norelax.

For the case of LS + SS\_norelax (solid blue), where the grid-scale and subgrid-scale dynamic components are both used and no relaxation is applied, the precipitation rates are underestimated for most domains except D200. For the case of LS + SS\_3hrelax (solid red), as for the LS cases, the precipitation rate is reduced for D300 when relaxation is applied. Relaxation tends to reduce the precipitation rate for the 300 and 200 km grid scales. For the smaller grid scales of 100 and 50 km, the impact of the relaxation is not clear.

A synthesis of the results from all four cases points to a tendency of the SCAM5 to underestimate precipitation rate more so as grid resolution increases below 200 km (i.e., as grid size decreases). This tendency might be associated with the MCS structure and its processes should not be viewed as a general conclusion. However, the results suggest that the sensitivity of the SCM simulation to grid size must be taken into account when attributing simulation errors to physical parameterization schemes.

Since the clouds simulated by SCMs are often sensitive to forcing [e.g., Fridlind *et al.*, 2012], we compare the performance of cloud simulations without relaxation applied to observations. Figure 6 shows the ARMBE cloud fraction during the time period for the SCM simulations. Two convective events corresponding to strong precipitation rate can be seen during 09:00 UTC to 15:00 UTC on 13 June and 03:00 UTC to 12:00 UTC on 14 June. We note that the observed cloud fractions are derived from the profiles of point observations, while the SCAM5 cloud fraction represents the average over a domain of a given grid size. Although a meaningful comparison between SCAM5 results with observations usually requires a sufficiently long observation period of the latter, the general characteristics of a large-scale phenomenon such as an MCS can be captured.

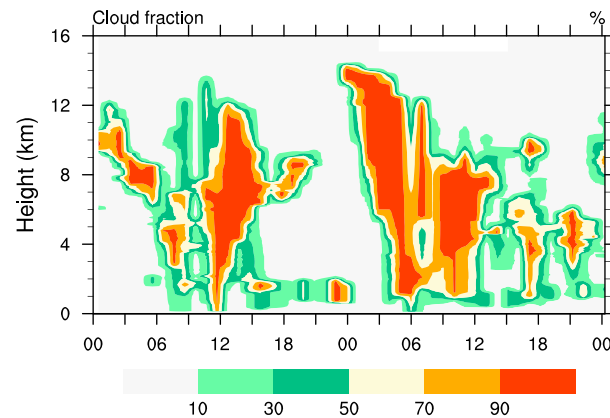


**Figure 6.** Time-height cross section of cloud fractional occurrence from the ARMBE over the ARM SGP central facility. Note that the ARMBE is temporally averaged for a single geographical point, and the x axis is in UTC time starting at 00:00 UTC on 13 June.

levels during the main precipitation event that occurs from 03:00 UTC to 12:00 UTC on 14 June. It is clear from Figure 5 that the simulated precipitation is less than one third of that observed, which could be related to vertical velocity. In Figures 2a1–2a4, the upward vertical velocities are associated with the main precipitation event for D300 and D200, but strong downward vertical velocities—as large as 0.3 m/s—occur in the lower troposphere for D100 and D50. It is unlikely that this strong downward vertical velocity is caused by the MS-DA system because it can simulate the precipitation rates well (Figure 5, gray lines), which suggests that its vertical velocities are reasonable. Therefore, the SCAM5 may be limited when dealing with strong vertical velocities associated with small grid scales such as D100 and D50.

## 5.2. Impact of the Subgrid-Scale Dynamic Component

The impact of the subgrid-scale dynamic component can be determined from the differences between the experiments that consider only the grid-scale component (Exp. LS) and those that use the grid-scale and subgrid-scale dynamic components (Exp. LS + SS). In Figure 5, we see that the subgrid-scale dynamic component reduces the precipitation rates for D300 but not for the grid scales smaller than 200 km. In terms of cloud fraction, the subgrid-scale dynamic component tends to increase middle- and low-level cloud fraction but reduce high-level cloud fraction for D300 and D200 (Figure 7), while it decrease middle- and low-level cloud fraction but increase high-level clouds for D100. For D50, the impact is minor.

## 5.3. Subgrid-Scale Dynamic Component Versus Relaxation

The relaxation terms in equations (1) and (2) have often been used in SCM simulations, but they are not independent of the subgrid-scale dynamic component as we pointed out in section 2. *Ghan et al.* [2000] showed that the impact of relaxation on SCM simulations tends to be mixed, either improving or degrading the SCM performance; thus, the role of the relaxation term needs to be further quantified. Since we have determined the subgrid-scale dynamic component, a direct comparison can be made between the impacts of relaxation and the subgrid-scale dynamic component.

Relaxation reduces precipitation rate for D300 and D200, as can be seen in Figure 5 by the difference between Exps. LS\_norelax and LS\_3hrelax and between LS + SS\_norelax and LS + SS\_3hrelax. The precipitation rate is halved during the main precipitation event on 14 June for D300. In section 5.2, we saw that the subgrid-scale dynamic component reduces precipitation as well, as can be seen from the difference between Exps. LS\_norelax and LS + SS\_norelax. For D300, the precipitation in Exps. LS\_3hrelax and LS + SS\_norelax is reduced by similar amount of  $\sim 1.0$  mm/h compared to Exp. LS\_norelax during the convective event. This result seems to suggest that in terms of precipitation, relaxation may play a role similar to the subgrid-scale dynamic component. We note that for the case of LS + SS\_3hrelax, where the subgrid-scale dynamic component and 3 h relaxation are applied, the precipitation rate largely drifts apart from the observation for

In Figure 7, we see that high clouds are overestimated for grid scales D300 and D200 (both of experiments (Exps.) LS and LS + SS), but this overestimation is significantly reduced for the smaller grid scales D100 and D50. This reduction of cloud fraction at higher altitudes is most evident around 21:00 UTC on 13 June. The observations show few high clouds during a period of about 6 h, from 18:00 UTC on 13 June to 00:00 UTC on 14 June. We conclude that the SCAM5 overestimates high clouds for all grid scales, but the overestimation is not significant for the small grid scales D100 and D50.

The SCAM5 simulations underestimate the lower level cloud fractions for all grid scales. For grid scales D100 and D50, in particular, cloud fraction does not extend to lower

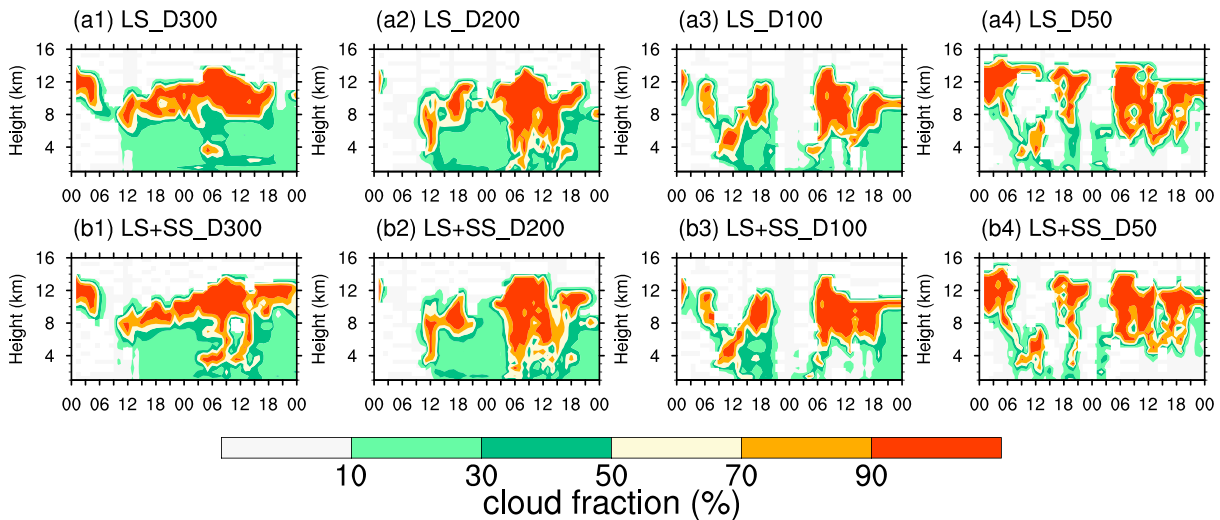


**Figure 7.** SCAM5-simulated cloud fraction for (a1 and b1) D300, (a2 and b2) D200, (a3 and b3) D100, and (a4 and b4) D50. The simulations in Figures 7a1–7a4 are driven with the large-/grid-scale forcing, and the simulations in Figures 7b1–7b4 are driven with the large-/grid- plus subgrid-scale dynamic forcing components. No relaxation was applied. Note that the x axis is in UTC time starting at 00:00 UTC on 13 June.

D300, but this drift is not seen at the smaller grid scales. One should be cautious when using relaxation when the subgrid-scale dynamic component is included.

For the cloud simulation, the impact of relaxation tells a different story. Subgrid-scale dynamics, without relaxation, often increases middle- and low-level cloud fraction (Figure 7), whereas relaxation tends to reduce middle- and low-level cloud fractions (compare Figure 8 to Figure 7). The impact of relaxation on cloud formation must be different from the mechanism responsible for precipitation reduction.

It is beyond the scope of this paper to attribute the precipitation reduction to specific microphysical processes; however, we hypothesize that the precipitation reduction caused by relaxation is related to the reduction of middle- and low-level clouds. Given that the impact on middle- and low-level clouds is opposite to the subgrid-scale dynamic component, caution should be exercised when using the subgrid-scale dynamic component with relaxation in SCMs.

## 6. Summary and Discussion

We have addressed scale-aware large-scale forcing, which refers to the large-scale forcing explicitly associated with grid-scale and subgrid-scale components. The grid-scale component of the forcing aims to account for the wide range of spatial resolutions of current GCMs, from an order of 100 km to finer resolutions of an order of 10 km [IPCC, 2013]. The grid-scale and subgrid-scale dynamic components are derived based on a multiscale data assimilation system with WRF at a cloud-resolving resolution of 2 km, which was applied to the ARM SGP region. Comprehensive SCAM5 experiments are conducted to examine the dependence on grid scale and sensitivity to the subgrid-scale dynamic component in terms of simulated precipitation and cloud fraction.

As expected, the large-scale forcing intensity and temporal variability increase as spatial scales are reduced. The increase is most pronounced during the MCS precipitation events. The SCAM5-simulated precipitation is overestimated for scales of about 200 km and reverses to be underestimated for smaller scales. The results indicate that spatial scale needs to be considered in the interpretation of SCM simulations.

The analyses show that the subgrid-scale dynamic component, the subgrid-scale flux divergence due to subgrid-scale dynamic processes, often provide significant horizontal advection for spatial scales larger than 200 km and is a nonnegligible component of the large-scale forcing. The subgrid-scale dynamic component has a beneficial impact on the SCAM5 simulations, especially for larger domains. Such results support our argument that the subgrid-scale dynamic processes are partially parameterized as hyperdiffusion in CAM5, and thus its inclusion enhances the consistency between the horizontal flux divergence and the vertical flux divergence that is accounted for in parameterizations.

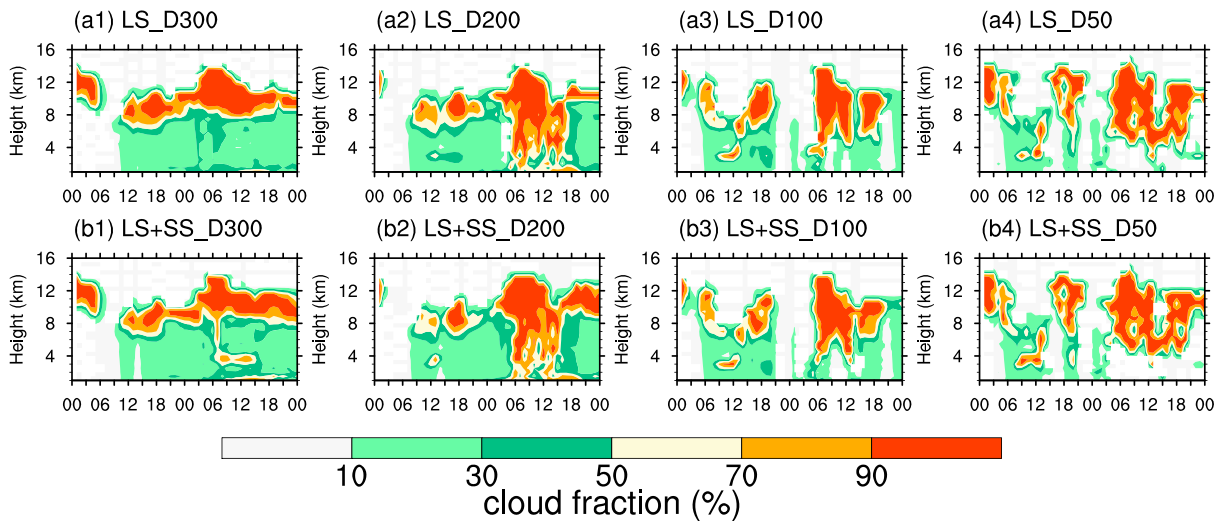


**Figure 8.** Same as Figure 7 but with 3 h relaxation applied. Note that the x axis is in UTC time starting at 00:00 UTC on 13 June.

The subgrid-scale dynamic component and relaxation are dynamically related [Randall and Cripe, 1999]. The impacts of the subgrid-scale dynamic component and relaxation in the SCAM5 are similar in terms of precipitation rate but not cloud fraction. This result agrees with the conclusion in Ghan et al. [2000] that the impact of relaxation may vary for different field variables.

We have shown that the subgrid-scale dynamic component is a significant component in large-scale forcing fields and that SCM simulations are sensitive to it. However, from the experiments presented, we cannot reach the conclusion that the inclusion of subgrid-scale dynamic component improves the SCM simulation from the experiments that are presented. This is because the SCM responds to the subgrid-scale dynamic component in a complex way.

**Acknowledgments**

The research described in this publication was supported by the U.S. Department of Energy Earth System Modeling program via the FASTER project (<http://www.bnl.gov/faster>). This research was carried out, in part, at the Jet Propulsion Laboratory, California Institute of Technology, under a contract with the National Aeronautics and Space Administration (NASA). The authors are grateful to Ann Fridlind (NASA Goddard Institute for Space Studies) and Leo J. Donner (Geophysical Fluid Dynamics Laboratory) for stimulating the discussions and insightful suggestions. Data from the U.S. Department of Energy’s SGP ARM Climate Research Facility (<http://www.arm.gov/>) are used in this article. The authors thank the anonymous reviewers for their comments that were very helpful in improving the manuscript.

**References**

Ackerman, T. P., and G. M. Stokes (2003), The Atmospheric Radiation Measurement Program, *Phys. Today*, 56(1), 38–44.

Bechtold, P., et al. (2000), A GCMSS model intercomparison for a tropical squall line observed during toga-coare. II: Intercomparison of single-column models and a cloud-resolving model, *Q. J. R. Meteorol. Soc.*, 126(564), 865–888.

Betts, A. K., and M. J. Miller (1986), A new convective adjustment scheme. Part II: Single column tests using GATE wave, BOMEX, ATEX and arctic air-mass data sets, *Q. J. R. Meteorol. Soc.*, 112(473), 693–709.

Buizza, R., M. Milleer, and T. N. Palmer (1999), Stochastic representation of model uncertainties in the ECMWF ensemble prediction system, *Q. J. R. Meteorol. Soc.*, 125(560), 2887–2908.

Clothiaux, E. E., T. P. Ackerman, G. G. Mace, K. P. Moran, R. T. Marchand, M. A. Miller, and B. E. Martner (2000), Objective determination of cloud heights and radar reflectivities using a combination of active remote sensors at the ARM CART sites, *J. Appl. Meteorol.*, 39(5), 645–665.

Clothiaux, E. E., et al. (2001), The ARM Millimeter Wave Cloud Radars (MMCRs) and the Active Remote Sensing of Clouds (ARSCL) Value Added Product (VAP), *DOE Tech. Memo. ARM VAP-002.1*, U.S. Department of Energy, Washington, D. C.

Fridlind, A. M., et al. (2012), A comparison of TWP-ICE observational data with cloud-resolving model results, *J. Geophys. Res.*, 117, D05204, doi:10.1029/2011JD016595.

Gettelman, A., H. Morrison, and S. J. Ghan (2008), A new two-moment bulk stratiform cloud microphysics scheme in the community atmosphere model, version 3 (CAM3). Part II: Single-column and global results, *J. Clim.*, 21(15), 3660–3679.

Gettelman, A., X. Liu, S. J. Ghan, H. Morrison, S. Park, A. J. Conley, S. A. Klein, J. Boyle, D. L. Mitchell, and J.-L. F. Li (2010), Global simulations of ice nucleation and ice supersaturation with an improved cloud scheme in the Community Atmosphere Model, *J. Geophys. Res.*, 115, D18216, doi:10.1029/2009JD013797.

Ghan, S., et al. (2000), A comparison of single column model simulations of summertime midlatitude continental convection, *J. Geophys. Res.*, 105(D2), 2091–2124, doi:10.1029/1999JD900971.

Hoskins, B., T. N. Palmer, and G. Shutts (2004), Stochastic physics. European Centre for Medium-Range Weather Forecasts. [Available at [http://www.ecmwf.int/about/special\\_projects/hoskins\\_stochastic\\_physica/report\\_2005.pdf](http://www.ecmwf.int/about/special_projects/hoskins_stochastic_physica/report_2005.pdf)].

Houze, R. A. (2004), Mesoscale convective systems, *Rev. Geophys.*, 42, RG4003, doi:10.1029/2004RG000150.

Intergovernmental Panel on Climate Change (IPCC) (2013), *Climate Change 2013: The Physical Science Basis. Contribution of Working Group I to the Fifth Assessment Report of the Intergovernmental Panel on Climate Change*, 1535 pp., Cambridge Univ. Press, New York.

Li, Z., S. Feng, Y. Liu, W. Lin, M. Zhang, T. Toto, A. M. Vogelmann, and S. Endo (2014), Development of fine-resolution analyses and expanded large-scale forcing properties. Part I: Methodology and evaluation, *J. Geophys. Res. Atmos.*, doi:10.1002/2014JD022245.

Mather, J. H., and J. W. Voyles (2013), The ARM Climate Research Facility: A review of structure and capabilities, *Bull. Am. Meteorol. Soc.*, 94, 377–392.

Morrison, H., and A. Gettelman (2008), A new two-moment bulk stratiform cloud microphysics scheme in the Community Atmosphere Model, version 3 (CAM3). Part I: Description and numerical tests, *J. Clim.*, 21(15), 3642–3659.

- Neale, R. B., et al. (2010), Description of the NCAR Community Atmosphere Model (CAM 5.0), *Tech. Note NCAR/TN-486+STR*, Natl. Cent. for Atmos. Res., Boulder, Colo.
- Ooyama, K. V. (1987), Scale-controlled objective analysis, *Mon. Weather Rev.*, *115*(10), 2479–2506.
- Palmer, T. N. (2001), A nonlinear dynamical perspective on model error: A proposal for non-local stochastic-dynamic parametrization in weather and climate prediction models, *Q. J. R. Meteorol. Soc.*, *127*(572), 279–304.
- Petch, J. C., and J. Dudhia (1998), The importance of the horizontal advection of hydrometeors in a single-column model, *J. Clim.*, *11*(9), 2437–2452.
- Randall, D., and D. Cripe (1999), Alternative methods for specification of observed forcing in single-column models and cloud system models, *J. Geophys. Res.*, *104*(D20), 24,527–24,545, doi:10.1029/1999JD900765.
- Randall, D., et al. (2003), Confronting models with data: The GEWEX Cloud Systems Study, *Bull. Am. Meteorol. Soc.*, *84*(4), 455–469.
- Shutts, G. (2001), Some Interpretations of stochastic physical parameterizations, in *ECMWF Proceedings: Key Issues in the Parameterization of Subgrid Physical Processes 3–7 September 2001*, pp. 111–126, European Centre for Medium-Range Weather Forecasts Shinfield Park, Reading, U. K.
- Song, H., W. Lin, Y. Lin, A. B. Wolf, R. Neggers, L. J. Donner, A. D. Del Genio, and Y. Liu (2013), Evaluation of precipitation simulated by seven SCMs against the ARM observations at the SGP site, *J. Clim.*, *26*(15), 5467–5492.
- Stokes, G. M., and S. E. Schwartz (1994), The Atmospheric Radiation Measurement (ARM) Program: Programmatic background and design of the cloud and radiation test bed, *Bull. Am. Meteorol. Soc.*, *75*(7), 1201–1221.
- Xie, S., R. T. Cederwall, and M. Zhang (2004), Developing long-term single-column model/cloud system-resolving model forcing data using numerical weather prediction products constrained by surface and top of the atmosphere observations, *J. Geophys. Res.*, *109*, D01104, doi:10.1029/2003JD004045.
- Xie, S., et al. (2010), Clouds and more: ARM climate modeling best estimate data, *Bull. Am. Meteorol. Soc.*, *91*(1), 13–20.
- Zhang, M. H., and J. L. Lin (1997), Constrained variational analysis of sounding data based on column-integrated budgets of mass, heat, moisture, and momentum: Approach and application to ARM measurements, *J. Atmos. Sci.*, *54*(11), 1503–1524.